

See discussions, stats, and author profiles for this publication at: <https://www.researchgate.net/publication/261596408>

Gasification of Miscanthus x giganteus in an Air-Blown Bubbling Fluidized Bed: A Preliminary Study of Performance and Agglomeration

ARTICLE in ENERGY & FUELS · FEBRUARY 2014

Impact Factor: 2.79 · DOI: 10.1021/ef4022152

CITATIONS

3

READS

44

7 AUTHORS, INCLUDING:



[Alen Horvat](#)

University of Limerick

7 PUBLICATIONS 8 CITATIONS

[SEE PROFILE](#)



[Zhonglai Li](#)

University College Cork

22 PUBLICATIONS 507 CITATIONS

[SEE PROFILE](#)



[Stephen Dooley](#)

University of Limerick

49 PUBLICATIONS 909 CITATIONS

[SEE PROFILE](#)



[James J Leahy](#)

University of Limerick

76 PUBLICATIONS 1,273 CITATIONS

[SEE PROFILE](#)

Gasification of *Miscanthus x giganteus* in an Air-Blown Bubbling Fluidized Bed: A Preliminary Study of Performance and Agglomeration

Gang Xue,[†] Marzena Kwapinska,^{*,‡} Alen Horvat,[†] Zhonglai Li,[†] Stephen Dooley,[†] Witold Kwapinski,[†] and James J. Leahy[‡]

[†]Carbolea Research Group, Department of Chemical and Environmental Sciences, University of Limerick, Limerick, Ireland

[‡]Competence Centre for Biorefining and Biofuels, University of Limerick, Limerick, Ireland

ABSTRACT: Gasification of *Miscanthus x giganteus* (MxG) was conducted in an air-blown bubbling fluidized bed (BFB) gasifier using magnesite as bed material and a moderate rate of biomass throughput (246.82–155.77 kg/m²h). The effect of equivalence ratio (ER) (0.234–0.372) and bed temperature (645–726 °C) on the performance of gasification was investigated. The results reveal that MxG is a promising candidate for energy production via BFB gasification; of the conditions tested, the optimal ER and temperature are approximately 0.262 and 645 °C, where no sign of agglomeration was found. The product gas from this condition has a higher heating value of 6.27 MJ/m³, a gas yield of 1.65 N m³/kg_{biomass} (39.5% of CO and 18.25% of H₂ on N₂ free basis), a carbon conversion efficiency of 94.81% and a hot gasification efficiency of 78.76%. Agglomeration was observed at some higher temperature conditions and believed to be initiated by the formation of fuel-ash derived low melting temperature K-rich (potassium) silicates (amorphous material that cannot be detected by XRD). It is suggested that relatively low temperature (650 °C) needs to be used for the gasification of MxG to avoid potential agglomeration.

1. INTRODUCTION

Demand for energy coupled with the environmental effects arising from anthropogenic activities related to production and conversion of carbonaceous fuels is stimulating interest in alternative energy systems. Fossil fuels still dominate energy consumption, with a market share of 87%; while, renewable energy continues to make progress, but currently accounts for ~2% of global energy consumption.¹ The potential of biomass to provide an alternative sustainable source of carbon is becoming widely recognized, as it is considered carbon neutral. However, all biomass feedstock's share the same drawbacks, such as low bulk density, low energy density, and nonuniform physical and chemical properties, which limit their utilizations. Biomass, especially from herbaceous plants, tends to have high ash content, composed primarily of silicon, potassium, sodium, and alkali earth metals, which can restrict their use at high temperatures.²

Primarily based on the perceived simplicity of operation and commercial maturity of the pertinent technologies, direct combustion is currently the favored choice for the production of heat and power from lignocellulosic feedstocks. Alternatives to direct combustion, which have been reported to have relatively high energy efficiencies and improved environmental performance, include gasification and pyrolysis. Gasification is a relatively mature thermochemical conversion technology for carbonaceous material such as coal, whereby the feedstock is exposed to high temperatures (usually around 750–1100 °C in a fluidized bed) under substoichiometric oxidizing conditions (air or steam as gasifying agents) producing a combustible gas comprising primarily CO, H₂, CH₄, N₂, and CO₂. This gas, often referred to as "syngas", can be burned directly in boilers. The application of gasification technologies to biomass

feedstocks requires different processing parameters, in particular lower temperatures are necessary in order to mitigate the problems arising from ash softening and melting. Due to the inherent advantages of low process temperatures, isothermal operating conditions, and fuel flexibility, fluidized beds have been found to be among the most suitable approaches for thermochemical conversion of a wide range of biomass fuels.³ The bubbling fluidized bed (BFB) is the simplest and probably the most cost-effective concept for continuous biomass gasification. BFBs are flexible to a wide variety of biomass with various particle sizes. They provide a high rate of heat transfer between bed material and fuel and can exhibit a highly uniform temperature distribution throughout the reactor.⁴ However, a particular disadvantage of the fluidized bed is the risk of bed agglomeration, particularly when the ash of the feedstock is abundant in alkali metals.

Biomass energy crops such as miscanthus are becoming widely cultivated across Europe, as is Bamboo in Brazil.⁵ The most common miscanthus species currently commercially grown is *Miscanthus x giganteus* (MxG), due to its rapid growth, low mineral content, high biomass yield, and favorable efficiency on carbon capture.⁶ The number of publications reporting gasification of MxG is modest. Michel et al.⁷ conducted steam gasification of MxG using olivine based catalysts. They came to the conclusion that MxG is a good candidate for the production of syngas and its product gas quality is comparable to that produced from other biomass (almond shells, apricot stones, straw, and pine sawdust). The

Received: November 8, 2013

Revised: January 14, 2014

Published: January 14, 2014

Table 1. Properties and Ash Composition of Miscanthus (*Miscanthus x giganteus* MxG)

	ECN Phyllis database				miscanthus ash composition (wt %)	
	willow (#345)	poplar (#700)	corn stove (#704)	misanthus		
proximate analysis (wt %, as received)						
moisture	43.50	4.80	6.06	9.69	Na	1.42
volatile matter	47.12	80.99	75.96	82.33	Mg	3.9
ash	0.90	1.16	4.75	4.04	Al	0.55
fixed carbon (calculated)	8.48	13.05	13.23	3.94	Si	40.87
ultimate analysis (d.a.f)					P	3.29
C	51.00	50.03	49.31	47.63	S	3.74
H	6.00	6.07	6.04	6.19	Cl	1.4
N	0.10	0.23	0.70	0.40	K	27.34
S	n.a.	0.05	0.11	n.a.	Ca	14.22
O	42.90	43.60	43.56	45.78	Mn	0.33
total (with halides)	100	100	100	100	Fe	1.85
gross calorific value (MJ/kg)	18.86 (d.a.f)	19.74 (d.a.f)	19.06 (d.a.f)	18.36 (d)	total	98.92
chemical composition analysis (wt %) as received						
lignin	n.a.	n.a.	n.a.	21.62		
cellulose	n.a.	n.a.	n.a.	41.44		
hemicellulose	n.a.	n.a.	n.a.	21.04		

biomass flow rate in their study was rather low (0.48 kg/h) compared to the scale of the gasifier (100 mm inner diameter (ID)), as the emphasis in their study was not on the actual production of energy but on catalyst performance. Smoliński and co-workers⁸ steam gasified three different energy crops (MxG, Salix Viminalis, and Andropogon Gerardi) in a quartz tube (a fixed bed reactor) at atmospheric pressure and temperatures between 650–900 °C. The biomass was first pyrolyzed in an inert atmosphere before the desired temperature was reached and then the gasification medium was injected into the reactor where the biochar was gasified. This study was aimed at determining the reactivity of different energy crops. The reactivity was defined as the propensity of the biomasses to undergo thermochemical transformations.⁸ The authors concluded that the biochar of MxG showed the highest reactivity among all the feedstocks they tested. Chen et al.⁹ carried out air gasification of MxG in a circulating fluidized bed. The heating value and yield of product gas was around 4 MJ/Nm³ and 2 N m³/kg respectively, at an equivalence ratio of 0.3 and a temperature of 753 °C in the riser.⁹ Kallis et al.¹⁰ gasified MxG pellets in a downdraft gasifier and found that the distribution of heat and the resulting temperature distribution had a significant effect on the quality and quantity of the gas produced. Siedlecki et al., compared different biomass (clean wood, demolition wood, miscanthus, and Dutch straw) and bed material (sand, olivine, and magnesite) in a 100 kW thermal input steam–oxygen blown CFB gasifier.¹¹ It was concluded that the gasification of miscanthus on a magnesite bed gave a higher volume fraction of H₂, which may be attributed to special catalytic properties of miscanthus ash.

In fluidized bed gasification applications, quartz sand is widely used as a bed material due to its natural abundance and low cost. However, its drawback is that silica can react with alkali metals from the biomass ash and induce agglomeration with consequent defluidization in gasifiers.¹² In order to counteract the in-bed agglomeration problem, additives may be used with alkali-rich fuels.¹³ If the ash content of the fuel is high, extensive extraction of bed material is necessary to maintain the process pressure (bed inventory). Liliedahl et al.¹⁴ evaluated 145 gasification tests using eight different biomass

fuels (olive pomace, wheat straw, birch stem, reed canary grass, willow, miscanthus, and lucerne) and three bed materials (quartz sand, olivine, and magnesite). They analyzed the data by a multivariate statistical approach and concluded that the defluidization temperature when using magnesite was at least 150 °C higher than when using sand. Siedlecki et al.¹¹ gasified clean and demolition wood, miscanthus, and Dutch straw in a circulating fluidized bed gasifier using quartz sand, treated and untreated olivine, and magnesite as bed materials. They reported that magnesite had a positive impact on agglomeration prevention for fuels containing alkali and chlorine in the ash. Basile et al.¹⁵ used the same gasification facility (as Siedlecki et al.¹¹) to investigate steam reforming of the hot gas from gasified wood and miscanthus. They used magnesite as the bed material to avoid agglomeration as they stated the alkali metals from the biomass ash can react with silica present in other bed material (sand and olivine).

Although gasification of miscanthus in an air-blown BFB gasifier itself is not new, the detailed investigation of process conditions from the point view of energy production and gasification performance, present a valuable contribution to the scientific literature. Thus, the emphasis of the present work is to (1) study the performance of crushed miscanthus pellets in an air-blown BFB using a relatively high biomass feeding rate in order to evaluate its feasibility as a feedstock for energy production; (2) investigate the characteristics of magnesite as a bed material when the feedstock, characterized by high alkali and silica content, is used; (3) undertake a preliminarily investigation of the tendency of agglomeration.

2. EXPERIMENTAL METHODOLOGY

2.1. Biomass and Bed Material Characterization. The biomass feedstock used in this study, MxG, originates from Adare, Ireland, and was pelletized by JHM Crops, Ireland. Detailed information regarding the composition of the miscanthus used has been already been reported.¹⁶ In this study, it was received as pellets (6 mm outside diameter with an average length of 170 mm). In order to facilitate the biomass feeding, the pellets were crushed to dimensions smaller than 5 mm in diameter. The properties of the raw MxG and its ash composition are presented in Table 1. It was compared to other feedstocks from the ECN Phyllis database, which are used for

gasification including willow (#345), poplar (#700), and corn stover (#704). The proximate analysis was conducted according to BS EN 14774-1:2009 (moisture content), BS EN 14775:2009 (ash content) and BS EN 15148:2009 (volatile matter content). Raw biomass was prepared for the analysis of chemical composition according to the following standards: D 1150-96 (preparation of extractive free biomass), D 1107-96 (ethanol-toluene solubility of biomass), and E1757-01 (preparation for compositional analysis). It can be seen that the properties of MxG, for instance gross calorific value and ultimate analysis (d.a.f.), are similar to those of other feedstocks. However, there is an obvious difference with respect to the proximate analysis, especially in the case of ash and moisture content. Acid hydrolysis was conducted according to the NREL (National Renewable Energy Laboratory) analytical procedure,¹⁷ and ash content and volatile matter content are expressed on a dry basis. Fixed carbon content was calculated according to Basu.¹⁸ Ash composition analysis was conducted by scanning electron microscope-energy dispersive X-ray spectroscopy (SEM/EDS), and the results presented are based on the average composition of 34 randomly selected locations.

Considering the high alkali content of the biomass tested, especially that of potassium, magnesite was chosen as the bed material in this study to reduce agglomeration related problems. As magnesite contains no silica, it is considered as an antiagglomeration bed material that will delay the initiation of agglomeration. This naturally occurring mineral, magnesite (DB 90) was supplied by MINELCO, U.K.; size separated using a series of sieves to particles in the range 355–600 µm, with a mean particle size of 472 µm, 3043 kg/m³ absolute particle density, and 1381.7 kg/m³ bulk density. The chemical composition of the bed materials was analyzed by SEM-EDS and is presented in Table 2.

Table 2. Chemical Composition of Magnesite DB90 (mass fraction wt %)

spectrum	O	Mg	Ca	Fe	total
1	46.73	51.63	0.85	0.79	100
2	48.12	50.14	1.06	0.68	100
3	48.19	49.13	1.89	0.79	100
4	47.74	50.79	0.88	0.59	100
mean	47.69	50.42	1.17	0.71	100
std. dev.	0.68	1.06	0.49	0.1	
max.	48.19	51.63	1.89	0.79	
min.	46.73	49.13	0.85	0.59	

2.2. Experimental Setup. A pilot scale air-blown bubbling fluidized bed gasifier (BFBG) located at the University of Limerick was used in this study. A schematic diagram of the BFBG is shown in Figure 1. The system essentially consists of six sections: biomass feeding system, fluidized bed reactor, air and steam delivery and heating system, tar sampling system, downstream cleaning section, and product gas analysis section.

The vertical reactor section is 3300 mm in height and fabricated from stainless steel (316L). It is divided into a bed section (1750 mm high and 134.5 mm inner diameter (ID)) and freeboard section (1250 mm high with an ID of 211.6 mm). Three independent electrical heating zones cover the reactor, each consisting of a furnace and insulating jacket. The gasification agent, air, is supplied by an external compressor and is introduced at the bottom of the reactor. A stainless steel mesh is installed at the base of the gasifier as an air distributor. Solid fuel is fed at the bottom of the fluidized bed (190 mm above the distributor plate) by means of two feeding screws.

In order to monitor the reactor temperature, nine Type-K thermocouples (TC Ltd., U.K.) are positioned in the reactor at the locations marked in Figure 1. Temperature indicators and controllers (TIC) are used for temperature measurement and control; temperature indicator (TI) is used for temperature measurement only. Specifically, TIC02 is located in the chamber underneath the air distributor to determine and control the temperature of the gasifying

air; three thermocouples, namely TI05, TI06, and TIC08, are installed in the bed zone and located 205, 555, and 755 mm above the air distributor, respectively. Additionally, for safety, two alarm thermocouples are placed in both bed and freeboard zones. Pressure indicators (PI) 01 and 02 are respectively located at the base and top of the reactor. An independent differential pressure sensor was used to monitor differential pressure changes. In addition, the downstream system (after the main reactor) is also controlled and monitored by thermocouples and pressure sensors.

2.3. Experiment Procedure. **2.3.1. Gasification Procedure.** The minimum fluidization velocity was determined prior to the gasification tests. The detailed procedure is as follow: the gasifier was loaded with 6.6 kg of bed material and heated to 540 °C (TIC06) after which the air flow was increased gradually. Correspondingly, the differential pressure in the bed was increased until the minimum fluidization was reached in the bed, at which point the differential pressure decreased slightly and fluctuated within a certain range with the increase of air flow. The result shows that an air feeding rate of 53 Ndm³/min was able to fluidize the bed at 550 °C. The air velocity at such condition calculated according to Wen and Yu, eq 1,¹⁹ is 0.134 m/s.

$$U_{mf} = \frac{\mu}{D_v \rho} \left\{ \left[(33.7)^2 + 0.0408 \frac{D_v^3 \rho (\rho_p - \rho) g}{\mu^2} \right]^{1/2} - 33.7 \right\} \quad (1)$$

where, U_{mf} , μ , D_v , ρ , ρ_p and g represent the minimum fluidization velocity, viscosity of fluid media, volumetric diameter of bed material, density of fluid media, absolute density of bed material, and acceleration due to gravity, respectively.

At the start-up of each experiment, 6.6 kg of bed material was loaded into the reactor, which corresponds to a bed height of 0.33 m at unfluidized conditions (above the center of biomass feeding screw) and a gas residence time of 2.5 s. Biomass feeding was started when the bed temperature was in the range 510–540 °C. The temperature of the reactor wall was supported by heating elements during gasification to minimize the heat loss and maintain the temperature in the gasifier. In order to maintain the fluidizing condition in the reactor and to keep the gas residence time relatively constant, a fixed air flow rate (53 Ndm³/min) was used in this study. The biomass feed rate was varied by changing the rotating speed of the agitator on the biomass hopper and screw feeders. The equivalence ratio (ER), defined as the ratio between the amount of O₂ fed to the gasifier and the O₂ needed for a complete stoichiometric combustion of a unit mass of biomass, was varied (0.234, 0.262, 0.281, and 0.372) by changing the biomass feed rate from 3.51 to 2.21 kg/h. In order to check consistency of the biomass feeding rate, a known amount of feedstock was loaded into the hopper before gasification, and after the experiment the biomass hopper was emptied. The biomass left in the hopper was weighed so as to calculate the mass of biomass actually consumed during the test. The biomass feeding rates presented in Table 3 were calculated as average values for the whole period of gasification.

The gasification reactor is followed by two cyclones, which are used to separate particulates from the gas stream. A secondary (catalytic) reactor after the cyclones was not used in the current study and was maintained at a temperature of 500 °C. Additionally, to protect the downstream analytic devices, two parallel filters were used to prevent fine particles and tar passing through the cleaning system.

At the end of each test, both air and biomass feeding was stopped. The reactor was flushed with N₂ gas allowing the system to cool to ambient temperature and the bed material was discharged from the reactor for analysis. The main operating conditions and results from six gasification experiments are summarized in Table 3.

2.3.2. Product Gas Analysis. The flow rate (kg/h) of product gas was measured by a Coriolis mass flow meter (Bronkhorst CORI-TECH) after the filters. The cleaned product gas was sampled after the mass flow meter and analyzed online by an Agilent Micro-GC 3000 equipped with three modules, each with a thermal conductivity detector configured for the detection of permanent gases and light hydrocarbons such as methane, ethane, ethylene, and acetylene.

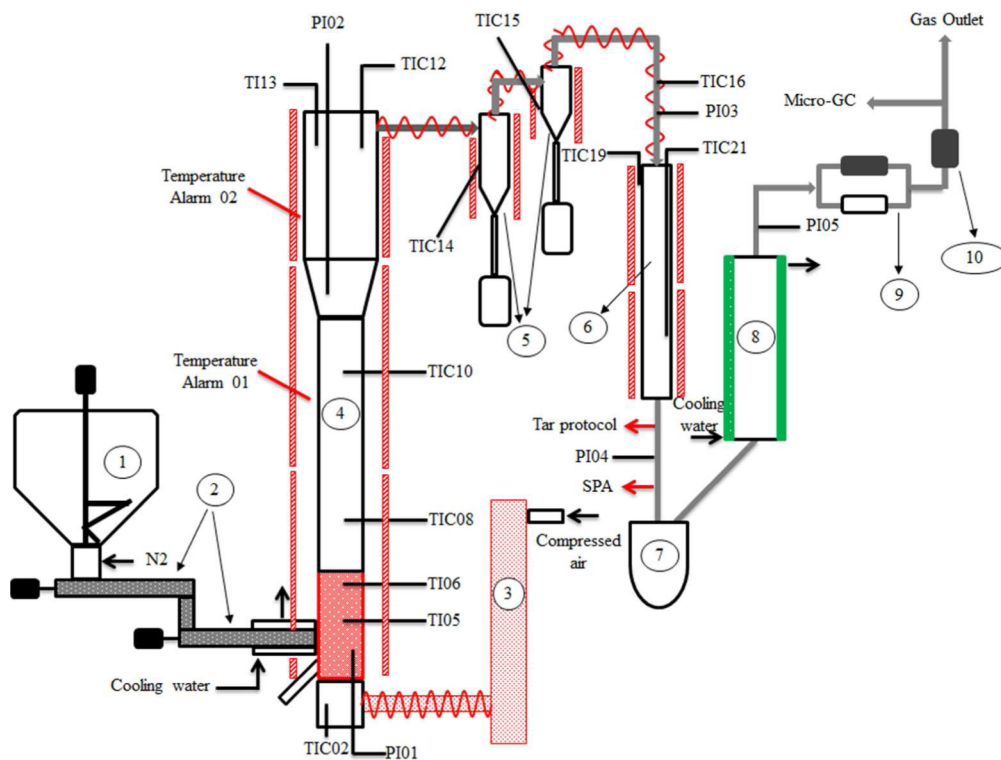


Figure 1. Bubbling fluidized bed gasifier at the University of Limerick: (1) 280 dm³ biomass hopper; (2) feeding screws; (3) air preheater; (4) gasifier reactor; (5) cyclones; (6) catalytic reactor; (7) tar trap; (8) heat exchanger; (9) downstream filters; (10) mass flow meter.

Table 3. Main Parameters Used in Gasification Experiments and the Corresponding Results

	test 1	test 2	test 3	test 4	test 5	test 6
gasification temp., TI06, (°C)	639	645	693	723	700	726
biomass flow rate (with moisture) (kg/h)	3.51	3.14	2.93	2.21	3.15	3.14
air flow rate (Ndm ³ /min)	52.55	52.66	52.66	52.66	52.99	52.99
bed material loaded (kg)	6.6	6.6	6.6	6.6	6.6	6.6
ER	0.234	0.262	0.281	0.372	0.263	0.264
defluidization	NO	NO	NO	NO	yes, larger clinkers	yes, large clinkers
flow rate of the produced gas with N ₂ (kg/h)	5.58	6.0	5.5	5.5	5.5	5.5
H ₂ (vol %)	7.5	9.95	9.5	9.6	9.1	8.8
CO (vol %)	11.2	21.5	16.9	10.6	18.2	17.3
CO ₂ (vol %)	18.7	18.2	18.7	17.95	18.4	18.3
CH ₄ (vol %)	4.2	3.4	3.2	3.2	3.3	3.5
C ₂ H ₄ -ethylene (vol %)	2.3	1.3	1.62	2.0	1.5	1.6
C ₂ H ₆ -ethane (vol %)	NA	NA	0.00	NA	0.1	0.00
C ₂ H ₂ -acetylene (vol %)	0.3	0.20	0.2	0.2	0.2	0.15
N ₂ (vol %)	55.9	45.5	49.9	56.3	49.1	50.2
HHV product gas (MJ/m ³)	5.63	6.27	5.7	5.7	5.9	5.8
gas yield (Nm ³ /h) with N ₂	4.69	5.17	4.7	4.7	4.7	4.7
gas yield (Nm ³ /kg _{biomass}) with N ₂	1.34	1.65	1.6	2.1	1.5	1.5
energy production (MJ/kg _{biomass}) HHV	7.54	10.35	9.3	11.1	8.7	8.6

Module A was fitted with a Plotu column of 30 μm/32 μm/8 m and Pre Col: PLOTQ 10 μm/320 μm/1 m, using helium as the carrier gas, to analyze carbon dioxide, ethylene, ethane, and acetylene. Module C was fitted with Molsieve 12 μm/320 μm/10 m and Pro Col PLOTU 30 μm/320 μm/3 m columns, and used argon as the carrier gas, to separate and detect hydrogen, oxygen, nitrogen, methane, and carbon monoxide. Module B was not used during this study.

In order to ensure the accuracy of product gas analysis, the Micro-GC was calibrated with a standard gas mixture before each trial; sampling started together with biomass feeding to determine product gas composition. Approximately, 1.5 to 2 h was required for the gasification process to achieve a steady state once biomass feeding had

commenced. The average gas composition during steady state was calculated and presented as the gas composition for the gasification tests in this study (Table 3).

2.4. Gasification Efficiency.

To evaluate the efficiency of gasification processes, the following equations were employed:

Higher heating value of product gas, HHV_P (MJ/m³)¹⁸

$$\text{HHV}_P = (V_{\text{CH}_4} 39.82 + V_{\text{CO}} 12.63 + V_{\text{C}_2\text{H}_4} 63.41 + V_{\text{H}_2} 12.74 + V_{\text{C}_2\text{H}_6} 70.29 + V_{\text{C}_2\text{H}_2} 58.26) / 100 \quad (2)$$

where V_{CO} , V_{H_2} , etc., are the volumetric percentage of the gas species in the product gas (vol. %);

Carbon conversion efficiency, η_C (%)²⁰

$$\eta_C(\%) = \frac{M_p[V_{CO} + V_{CO_2} + V_{CH_4} + 2(V_{C_2H_4} + V_{C_2H_6} + V_{C_2H_2})]}{M_B(1 - W_M)(1 - W_A)C\%} \quad (3)$$

M_p , M_B , W_M , W_A , and $C\%$ are the product gas (kmol gas/kg_{biomass}) generating rate, mass of feedstock (kg), moisture content of biomass (wt %), ash content of biomass (wt %), and carbon content of feed stock (wt % from elemental analysis, dry and ash free basis), respectively;

Hydrogen conversion efficiency, η_H (%)²⁰

$$\eta_H(\%) = \frac{M_p[2(V_{H_2} + V_{C_2H_2} + V_{CH_4} + 2V_{C_2H_4})]}{M_B(1 - W_M)(1 - W_A)H\% + M_{moisture}} \quad (4)$$

where H% is the hydrogen content of biomass (dry basis) and $H_{moisture}$ represents the hydrogen contributed by moisture present in both biomass and air;

Cold gas efficiency, η_{CG} %¹⁸

$$\eta_{CG}(\%) = \frac{LHV_p \times Y_{productgas}}{LHV_{BIOMASS}} \times 100 \quad (5)$$

Hot gas efficiency, η_{HG} %¹³

$$\eta_{HG}(\%) = \frac{LHV_p \times Y_{productgas} + E_p}{LHV_{BIOMASS}} \times 100 \quad (6)$$

where $LHV_{BIOMASS}$ is lower heating value of biomass, LHV_p is lower heating value of product gas, $Y_{productgas}$ is the yield of product gas per mass unit of biomass, and E_p is the sensible heat of the product gas.

2.5. Agglomerates Analysis. In the event that a gasification test resulted in clinkers/agglomerates, these were discharged from the bed and analyzed by a Hitachi SU-70 scanning electron microscope for morphology characterization. A 15 kV accelerating voltage and a 15 mm working distance were selected for the microstructure examination. The elemental compositions of the neck part of clinkers were analyzed by Energy-dispersive X-ray spectroscopy (EDS). The crystalline phases of fresh magnesite, miscanthus ash and clinkers were examined by X-ray dispersive spectrum on a Philips X'Pert MPD XRD (Cu anode) with 45 kV and 15 mA.

3. RESULTS AND ANALYSIS

3.1. Effect of Equivalence Ratio on Gasification Performance. **3.1.1. Influence of Equivalence Ratio on the Bed Temperature.** It is well-known that the ER has a significant influence on the overall performance and efficiency of the gasification process. In this study, the ER was investigated in the range 0.23–0.37 (Tests 1–4); the biomass feed was adjusted between 2.21 and 3.51 kg/h with a constant air flow of 53 Ndm³/min. As expected, the temperature in the bed during gasification increased gradually with ER (Table 3). The bed temperature in a directly heated gasifier is controlled by the relative rate of exothermic and endothermic reactions that are regulated by ER. Thus, the bed temperature is the overall result of oxidizing and reducing reactions in the gasifier, only the surplus heat, which is more than that required by the endothermic reactions, results in an increase in the gasifier temperature. Gomez-Barea et al.,²¹ reported a linear temperature increase for air gasification of olive stone in a pilot scale bubbling-fluidized-bed (150 kWth), with no heating elements on the reactor-wall, which was only insulated.

3.1.2. Influence of ER on the Composition of Product Gas. The change of gas composition on a N₂ free basis together with the concentration of N₂ in the product gas as a function of ER is presented in Figure 2a. It can be seen that the concentration

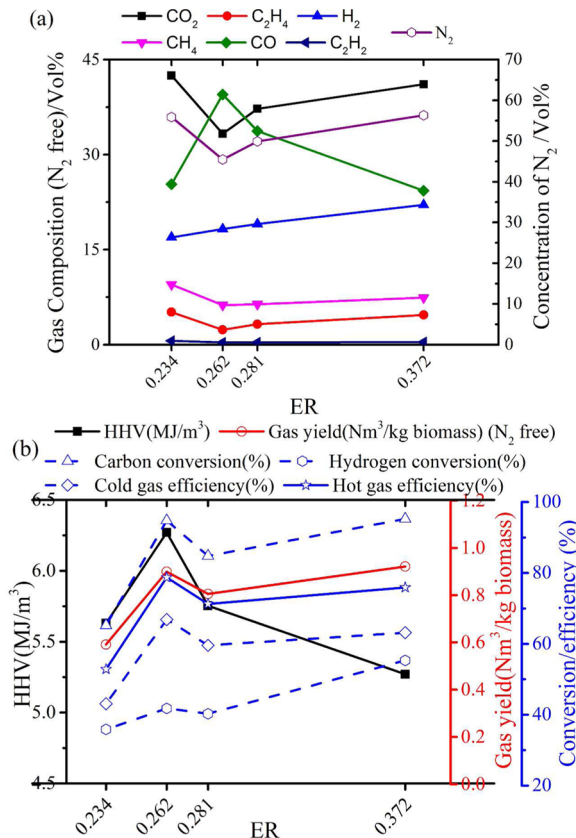


Figure 2. Effect of (a) ER on concentration of product gas and (b) ER on performance of gasification.

of CO, H₂, and CO₂ showed significant variations; while the amount of light hydrocarbons, namely methane, ethylene, and acetylene changed only slightly.

As observed, the concentration of N₂ is in the range 50–56%, except for experiment #2 where 45% was recorded. The fraction of CO increased initially and then decreased along with increased ER; whereas the content of H₂ increased progressively. The following set of main chemical reactions may be used to interpret the phenomenology of the gasification process:

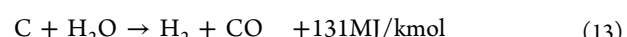
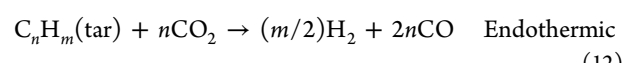
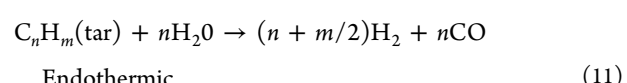
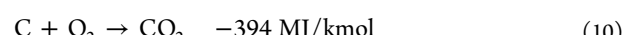


Table 4. Partitioned Volumetric Gas Yield on N₂ Free Basis (Nm³/kg_{biomass}) and Energy Yield (MJ/kg_{biomass}) versus ER

ER	gas yield (Nm ³ /kg _{biomass})						total gas yield, Nm ³ /kg _{biomass}	energy yield MJ/kg biomass
	CO ₂	C ₂ H ₄	H ₂	CH ₄	CO	C ₂ H ₂		
0.234	0.251	0.030	0.100	0.056	0.150	0.004	0.591	7.544
0.262	0.300	0.021	0.164	0.056	0.355	0.003	0.899	10.346
0.281	0.300	0.026	0.153	0.051	0.272	0.003	0.805	9.262
0.372	0.379	0.043	0.203	0.068	0.224	0.004	0.921	11.120



For the lowest ER (0.234), the low bed temperature (639 °C) limited the endothermic gasification reactions and the product gas shows low CO (25.35 vol %) and H₂ (16.93 vol %) content and high CO₂ content (42.5 vol %). As the ER was increased to 0.262, the amount of CO increased to its highest value of 39.5 vol %, while CO₂ decreased to its lowest concentration of 33.3 vol %. The increase in CO content can be attributed to the partial oxidation of carbon (eq 8) from the biomass, the water gas reaction 13, and the Boudouard reaction 7, which also induced the decrease of CO₂. Lahijani et al.²² gasified palm empty fruit bunches in the ER range 0.17–0.32 and reported similar results. When the ER was increased further to 0.372 the content of CO decreased from 39.5 vol % at 0.262 ER to 24.31 vol %. The main reason for the decrease of CO concentration is the increased stoichiometric O₂ supply which gives rise to oxidation reactions 10 and 14. It can be verified by the increased CO₂ concentration from 33.3 to 41.9%, when the ER increased from 0.262 to 0.372. An increase in H₂ is associated with the water gas shift reaction 9 at the cost of CO. Although higher temperatures have been demonstrated to improve product gas quality by increasing the gasification efficiency and tar cracking,²³ it can also degrade the product gas by oxidizing combustible gases into the undesirable CO₂ and H₂O. This can be seen by the increased CO₂ and N₂ concentration in the product gas when the ER was raised from 0.262 to 0.372. Kaewluan et al. gasified rubber wood chips in an air blown bubbling fluidized bed and investigated the effect of ER on the composition of product gas. They found that CO decreased with increasing ER, while H₂ increased initially up to an ER of 0.372 and then started to fall.²³

3.1.3. Influence of ER on the Gasification Performance.

The effect of ER on heating value, gas yield, and conversion efficiency is shown in Figure 2b. The higher heating value (HHV) of product gas was calculated from the gas composition and shows a similar tendency as that of CO. It increases initially from 5.63 MJ/m³ (ER = 0.234), reaches the highest value of 6.27 MJ/m³ (ER = 0.262) and is then followed by continuous decrease to 5.27 MJ/m³ at the highest ER = 0.372. Obviously, it is influenced by the concentration of combustible gas species in the product gas. The results obtained agree fairly well with an earlier study where dried sewage sludge was gasified in an air-blown BFB.²⁴

Gas yield is defined as the ratio of the mass flow rate of total N₂-free product gas to the mass flow rate of dry, ash-free biomass and is an important parameter for evaluating the performance of gasification processes. As depicted in Figure 2b, the gas yield increased initially, experienced a slight drop and went up again along with increasing ER. The increase at the beginning can be accounted for by the improved gasification efficiency induced by the increase of O₂ and the increased temperature via the following pathways: (a) improved biomass

pyrolysis²⁵ and gasification that gives more gas products; (b) tar cracking; (c) endothermic char gasification reactions.²⁶ It can be supported by the fact that carbon conversion peaked at an ER of 0.262 with values of 94.81%. The highest gas yield was observed for the highest ER, but its quality deteriorated, specifically the HHV dropped by 16% compared to that of ER = 0.262. This should be expected due to dilution with N₂ and increased rate of oxidation producing a higher fraction of CO₂. The large difference between carbon and hydrogen conversion is derived from the different mass fractions of C and H in the biomass; in addition, some H containing compounds, for example NH₃, H₂S, etc., are not measured. A slight decrease in gas yield was observed with the increase of ER, which may originate from the elutriation of biochar. The superficial gas velocity increased at higher temperature and accelerated the elutriation, which mitigated the positive effect of the higher temperature on the biomass conversion. However, for the case of the final increase at the highest ER, elevated biomass conversion may exert a dominant role. Because the data indicate that the mass of elutriated biochar did increase with the bed temperature, but the difference was too small to make a significant difference. On the other hand, the conversion efficiency of carbon dropped gently and then remained constant. This could be explained by the shortened residence time induced by higher bed temperature.²⁷ Hydrogen conversion increased, which might be influenced by the enhanced tar cracking and improved light hydrocarbon yield.

The overall energy efficiency of the gasification process is usually evaluated by its hot/cold gas efficiency. It can be seen that the cold/hot gas efficiency followed the same tendency as that of gas yield with the highest value of 66.89 and 78.76% respectively at an ER of 0.262. Undoubtedly, it is due to the combination of high gas yield and heating value of the product gas.

3.1.4. Influence of ER on the Absolute Gas and Energy Yield.

Since the ER was achieved by varying the biomass feeding rate at a fixed air flow rate, the mass flow rate of product gas is not representative of the effectiveness of the conditions in producing a valuable product. Thus the volumetric yield of each gas species on the basis of per unit mass of biomass (m³/kg_{biomass}) is regarded as more relevant from the point view of the application. The absolute volumetric yield of product gas is shown in Table 4. The highest yield of combustible gas is generated when the ER is 0.262, at which the highest and second highest amount of CO and H₂ were obtained, respectively.

The absolute energy yield (MJ/kg_{biomass}) of these four experiments calculated based on its gas yield (Nm³/kg_{biomass}) and HHV (MJ/m³) is also presented (Table 4). It can be seen that the highest energy yield is obtained from an ER of 0.372 with 11.11 MJ/kg_{biomass}, which is approximately 10% higher than the case of ER 0.262, 10.35 MJ/kg_{biomass}. Although the ER of 0.372 has a higher energy yield, it may not be considered to be the optimum ER in this study, since at this operating

condition the quantity of gas produced is the highest but its heating value is very low (Table 3). In addition, the C/H conversions, cold/hot gasification efficiencies, are lower than for ER = 0.262 (Figure 2b). Given the marginal (~10%) difference in gas yield, considering the factors presented above, the conclusion can be drawn that 0.262 is the optimum ER for this particular gasification installation, mode of operation and tested biomass.

3.2. Effect of Temperature on the Performance of Gasification. In order to examine the effect of bed temperature, another critical parameter, on the gasification of MxG, two more trials were carried out at higher bed temperature (700 and 726 °C) using the optimal ER (0.26) and the same air flow rate (53 Ndm³/min). The results of gas composition, HHV, C/H conversion and cold/hot gas efficiency are compared with optimum condition from the previous section and presented in Figure 3.

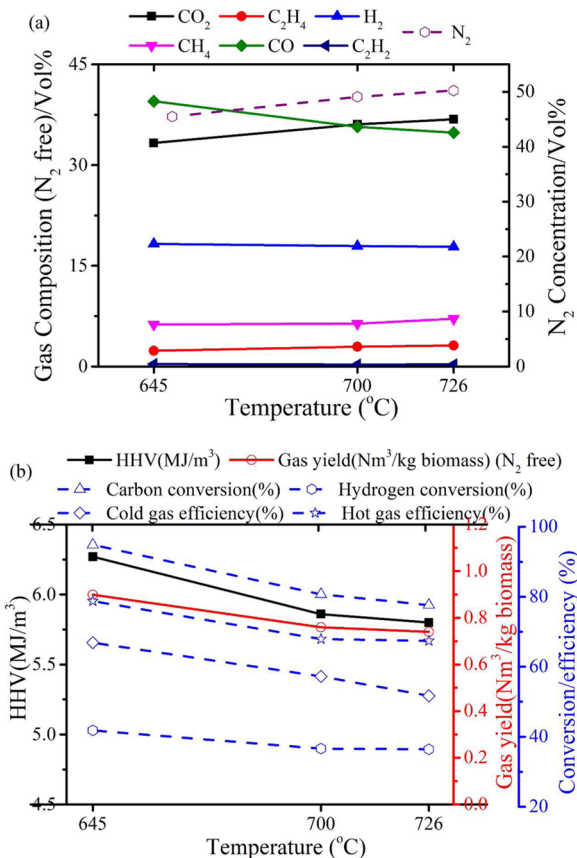


Figure 3. Effect of temperature on (a) concentration of product gas and (b) performance of gasification.

Figure 3a clearly shows that the quality of product gas was degraded with the increase in temperature. Among all the gas species, CO again showed the most obvious decrease from 39.5 to 34.8 vol %, while the concentration of CO₂ increases from 33.3 to 36.8 vol % and N₂ from 45.5 to 50.2 vol %. The content of H₂ and hydrocarbons did not change to the same extent at higher temperature (700 and 726 °C) in comparison with that of 645 °C. Consequently, HHV and cold/hot gas efficiency exhibited similar results with the concentration of CO. Lahijani et al. reported a similar trend in the temperature range of 650 to 750 °C when they used sawdust as a feedstock.²²

It should be noted that the gas yield as well as the C and H conversion efficiencies showed a slight drop with increased temperature (Figure 3b), which is different from the results of others. Lahijani and Zainal²² gasified empty fruit bunches from palm and also sawdust in an air blown bubbling fluidized bed and reported higher gasification efficiency, product gas yield, and carbon conversion efficiency when the temperature in the gasifier was increased. A possible overriding reason for this behavior, in addition to that described in section 3.1.3, is the agglomeration that was observed at 700 and 726 °C. As shown in Figure 4, large agglomerated “clinkers” were formed in the



Figure 4. Agglomerate, biochar, and biochar and bed material mixture discharged from gasifier after gasification: (a and b) from 700 °C gasification experiment 5; (c and d) from 726 °C gasification experiment 5; (e) biochar and bed material mixture from a test with good mixing in bed.

gasifier. Liliedahl et al.¹⁴ used magnesite as the bed material and reported sintering during their experiments, but they did not observe defluidization. Ross et al. reported a similar problem in their work.²⁸ In particular, for experiment #5, the clinker was sufficiently large to obstruct the whole reactor diameter (see Figure 4a), likely severely distorting the mixing and heat and mass transfer characteristics of the bed. The formation of clinkers could change the mode of mixing and cause air channeling, which allows the oxygen to escape from the gasification zone and oxidize the combustible gases in the freeboard instead of reacting with biochar in the dense bed. It has been found that the biochar in the gasifier was in the form of a fine powder (see Figure 4e) and no accumulation of biochar was observed after bed discharging if agglomeration did not occur; otherwise, the biochar did accumulate and was present as clusters in the bed (see Figure 4b and d), which not only reduces the contacting area between biochar and the gasification agent but also limits the mass and heat transfer. As a consequence, when agglomeration is observed to occur, the

overall gasification efficiency is likely to be lower than when the bed remains fluidized.

3.3. Mass Balance. In order to confirm the reliability of the measurements and investigate the fate of the main elements (C, H, O, and N) in the feedstock, a mass balance calculation (based on kg/h) is informative (eq 16).

$$MB_{\alpha} = \frac{\alpha_{\text{output}}}{\alpha_{\text{input}}} 100 \quad (16)$$

where MB is mass balance and α the mass of individual elements (C, H, O, and N, kg/h).

One gasification test (experiment #2, ER = 0.262, gasification temperature 645 °C) was used as a representative calculation for this study. An assumption, that there is no biochar accumulation in the bed is made to facilitate the calculation. All the data used in the calculation are the average values from the steady state during gasification, Table 3. The mass input is composed of air, feeding assisting N₂, and biomass, which may be accurately converted into elemental flow rates on the basis of the information provided in Tables 1 and 3. The products of gasification were split into four streams, including gas product, tar, moisture, and elutriated fine particulates. The elemental outputs of the product gas are calculated according to the gas compositions and flow rates reported in Table 3. The density and volume of gas species were taken at the condition of 15 °C and 1 atm. In the case of tar and elutriated fines, moisture and ash content analysis were first carried out; then, they were analyzed for elemental composition and calculated as kg/h.

The resulting mass balances for C, H, O, and N are 103.9, 78.4, 99.6, and 95.7%, respectively. The balance for H is lower than for the other elements, which show relatively good closure. The main reasons for lack of closure in the case of H are (1) the water content in the product gas is difficult to analyze accurately but expected to be significant and (2) a number of hydrogen rich compounds expected to be formed that were not measured in this study including ammonia, hydrogen sulfide, and some hydrocarbons such as benzene, toluene, xylene, etc. Data concerning material balances for gasification processes is poorly documented in literature. Frequently, the mass balance analysis is applied only to elemental carbon;²⁹ Siedlecki and co-workers published results showing material balances for all main elements C, H, N, and O.^{11,12} They also report the highest mass balance discrepancy for H.¹² The 95.7% recovery of nitrogen, which can be regarded to be chemically inert at the tested conditions, serves as an overall indication of the measurement uncertainty of this study.

3.4. Analysis of Clinkers. Considering the amount of silica, potassium, and sodium in the MxG ash, magnesite was selected as the bed material for this study to avoid any potential agglomeration because it had been reported as an agglomeration mitigating bed material.¹⁴ However, as discussed, the bed was observed to defluidize during gasification at certain higher temperature conditions. It should be acknowledged that the present study was not specifically designed to investigate the issue or mechanism of agglomeration. However, to date there are relatively few reports in the scientific literature on the sintering¹¹/agglomerating¹⁴ phenomena associated with magnesite where detailed information is scarce; thus, a preliminary study may be valuable.

3.4.1. Scanning Electron Microscope-Energy Dispersive X-ray Spectroscopy (SEM-EDS) Analysis. The clinkers discharged after gasification were analyzed by scanning electron micro-

scope-energy dispersive X-ray spectroscopy (SEM-EDS), Figure 5 and Table 5. The morphology of clinkers was not

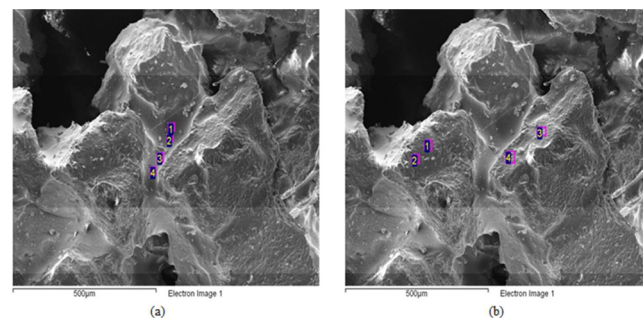


Figure 5. SEM images of an agglomerate from gasification: (a) neck; (b) coating on magnesite particles.

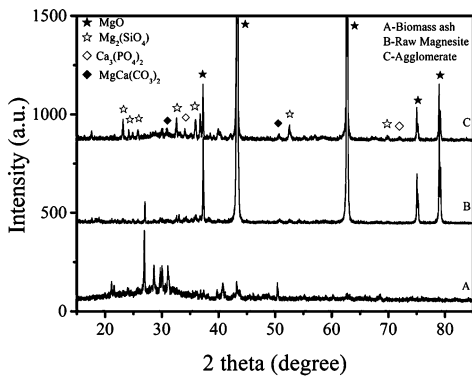
uniform. However, the EDS results indicate that the chemical composition of the necks formed between particles that join bed material particles together are quite similar. Accordingly, only two typical SEM images and their EDS results are presented here. Figure 5a suggests that several particles are bonded together, similar to observations made by other researchers.^{30–32} The corresponding EDS results indicate that the neck is mainly composed of Mg, Si, and K with smaller amounts of Ca, P, Al, and Na (Table 5a). Four spots were chosen and analyzed on the surface of bonded particles (Figure 5b and Table 5b). The particles were observed to be coated by layer of material of composition suggested to originate from the miscanthus ash. Other researchers reported a similar phenomenon.^{3,30,33} This surface layer consisted primarily of Mg, Si, and K as the major elements with lower concentrations of Na, Al, P, and Ca. It seems that the concentration of K on the surface of the bed material particles is lower than that of the neck areas, where the concentration of Mg is observed to be much higher. This can be explained by the fact that the coating layer is very thin allowing the X-ray to penetrate it and reach the magnesite particle which is mainly composed of MgO. This had been also observed by Öhman and co-workers.³ The concentration of Si, Ca, Al, and P on the surface of bounded particles and on the neck is comparable with the findings of Öhman et al.

3.4.2. X-ray Diffraction (XRD) Analysis. In order to identify which species were generated during the sintering reactions, the samples of raw magnesite, miscanthus ash and agglomerates were analyzed by XRD and the results are compared and shown in Figure 6. It was found that the spectrum of raw magnesite is mainly composed of five sharp peaks at $2\theta = 37.3^\circ, 43.3^\circ, 62.6^\circ, 75.1^\circ$, and 78.9° , indicating that its phase composition is essentially magnesium oxide (MgO, JCPDS 75-1525) while the spectrum of miscanthus ash is more complex making it difficult to identify all components only using XRD alone. However, when combined with the EDX results of biomass ash (Table 1), the presence of SiO₂ (JCPDS 47-0175; $2\theta = 21.1^\circ$ and 26.9°), K₂Mg(CO₃)₂ (JCPDS 33-1495) (not in the chart) and MgCa(CO₃)₂ (JCPDS 83-1766; $2\theta = 30.9^\circ$ and 50.7°) are confirmed.

It is obvious that the peaks for MgO still dominate the spectrum of the clinkers, but some peaks attributed to the ash are not present while new peaks are apparent. The newly identified compounds are Mg₂(SiO₄) with peaks at $2\theta = 23.1^\circ, 24.2^\circ, 25.8^\circ, 32.6^\circ, 35.9^\circ, 52.6^\circ$, and 69.8° (JCPDS 87-2044) and Ca₃(PO₄)₂ with peaks at $2\theta = 34.1^\circ$ and 71.9° (JCPDS 32-

Table 5. EDS Analysis of Agglomerates: (a) Neck Part; (b) Coating on Magnesite Particles

(a) mass fraction (wt %)								
spectrum	Na	Mg	Al	Si	P	K	Ca	total
1	2.44	13.95	1.4	40.08	3.46	30.74	7.92	100
2	2.67	14.23	1.58	40.27	3.47	29.94	7.85	100
3	2.82	13.93	1.5	38.21	3.22	32.34	7.96	100
4	2.72	14.47	1.4	40.16	3.44	29.51	8.3	100
mean	2.66	14.15	1.47	39.68	3.4	30.63	8.01	100
SD	0.16	0.25	0.09	0.98	0.12	1.25	0.2	
mole fraction (mol %)								
spectrum	Na	Mg	Al	Si	P	K	Ca	total
1	3.26	17.63	1.59	43.85	3.43	24.16	6.07	100
2	3.55	17.92	1.79	43.88	3.43	23.44	5.99	100
3	3.78	17.68	1.72	41.97	3.21	25.52	6.13	100
4	3.62	18.21	1.59	43.75	3.40	23.09	6.34	100
mean	3.56	17.86	1.67	43.36	3.37	24.05	6.13	100
SD	0.19	0.23	0.09	0.81	0.09	0.93	0.13	
(b) mass fraction (wt %)								
spectrum	Na	Mg	Al	Si	P	K	Ca	total
1	1.69	34.26	1.18	39.05	0.7	16.83	6.29	100
2	1.32	35.66	0.91	41.57	0.34	14.15	6.05	100
3	2.12	32.01	1.57	39.81	0.87	16.64	6.97	100
4	2.01	33.37	1.3	39.77	0.69	16.5	6.37	100
mean	1.79	33.83	1.24	40.05	0.65	16.03	6.42	100
SD	0.31	1.33	0.24	0.93	0.19	1.09	0.34	
mole fraction (mol %)								
spectrum	Na	Mg	Al	Si	P	K	Ca	total
1	2.08	39.96	1.24	39.42	0.64	12.21	4.45	100
2	1.61	41.18	0.95	41.55	0.31	10.16	4.24	100
3	2.63	37.49	1.66	40.35	0.80	12.12	4.95	100
4	2.48	38.92	1.37	40.14	0.63	11.96	4.51	100
mean	2.20	39.39	1.30	40.37	0.60	11.61	4.54	100
SD	0.39	1.36	0.25	0.77	0.18	0.84	0.26	

**Figure 6.** XRD analysis of (A) miscanthus ash; (B) raw magnesite; (C) agglomerates.

0176). The intensity of the peaks assigned to $\text{MgCa}(\text{CO}_3)_2$ increased in the case of agglomerates compared to that of ash, suggesting that some ash compounds reacted with bed material during gasification. XRD can only detect compounds in the crystalline form, and it is likely that there are other low melting point eutectics that exist as amorphous phases or as crystalline components too low in concentration to be detected, but which may play important roles in bed agglomeration. Lin and Wey³² gasified an artificial feedstock (composed of sawdust, polyethylene bag, alkali, and earth alkali metals) using silica sand as the bed material to investigate the effect of mineral composition

of waste and operating conditions on the particle agglomeration. They analyzed compounds at the connecting bridge of clinkers by XRD, and SiO_2 was found to be the dominant species. They explained that the eutectics in connecting bridges were too thin to be detected by XRD.

3.4.3. Bed Agglomeration. Several parameters, such as particle size and distribution of bed material, the bed geometry, pressure or humidity,³² have potential to significantly influence agglomeration. Temperature plays a key role due to the degree of sintering³⁴ and the amount of liquid phase eutectic³⁵ increases with temperature. Moreover, it is suggested that eutectics may migrate from particle to particle.³⁶ According to Bartels¹³ et al., agglomeration is difficult to predict because, although while reasonable control of process conditions is possible the chemical composition and behavior of the ash formed is fuel dependent and thus variable from feedstock to feedstock. The Si and K can form low-temperature melting species in the bed; these particulate species will probably continue to be enriched in K overtime, further reducing the melting temperature promoting sudden severe viscous flow agglomerations.³⁷ Lin et al.³² found that Mg and Ca have two opposite effects, namely inhibition or promotion, and the concentration of Na plays a very important role in the process. At low concentration of Na (~ 0.4%), addition of Mg and Ca significantly inhibited defluidization, because Mg and Ca reduced the generation of compounds with low melting points, and forming species materials with higher melting points. The

inhibiting effect of Mg and Ca rapidly decreased when the concentration of Na increased to 1.2%. However, when the concentration of Na was increased to 3.0%, adding Mg and Ca seemed to promote agglomeration. Biomass ash, on the other hand, is a multicomponent system of particulate material; it has several characteristic and measurable ash fusion temperatures, and thus, melting may occur over a wide temperature range.³⁸ The melting point of laboratory generated ash for analysis is quite different from that of ash collected from a gasifier, a possible reason why agglomeration can occur at temperatures lower than its melting point.

Combining the analysis of SEM-EDS and XRD, it is probable that the agglomeration was mainly initiated by the formation of fuel-ash derived low melting-temperature, K-rich, silicates (amorphous material that cannot be detected by XRD).

Apart from the operating parameters used for gasification, the gasifier design has a critical influence on the fluid dynamics of bed material during gasification, especially the air distributor. As mentioned in section 2.2, a stainless steel mesh was used as the air distributor, which was fabricated from thin steel wires. The size of the square orifices was very small but its number was large, which means it had relatively big opening area. As a result, the pressure drop across the grid was relatively low. The low pressure drop probably gave rise to nonuniform fluidization according to Basu.²⁰ However, the negative effects of a large opening area can be offset by a high air feeding rate.²⁰ Whether the air flow was sufficiently high to diminish the negative effects of the opening area of the air distributor and to what extent the low pressure drop across the grid aided the agglomeration still needs to be investigated.

4. CONCLUSIONS

Fluidized bed gasification of miscanthus was investigated to identify the effect of equivalence ratio and temperature on the gasification performance.

- (1) Air-blown gasification of MxG yields 1.35 to 2.11 N m³/kg_{biomass} of producer gas with a lower heating value of between 4.87 and 5.88 MJ/m³. There is an overall increase of conversion efficiency and gas yield with an increase in equivalence ratio.
- (2) The effect of temperature is masked by that of bed agglomeration. Since grassy biomass is characterized by relatively high silica, potassium and sodium content, agglomeration was observed even at low gasification temperatures. This behavior should be considered before large scale applications are deployed.
- (3) The agglomeration was induced by the accumulation of low melting point eutectics that originated from the alkali-metal-rich biomass ash. In order to make it possible to use this combination (miscanthus and magnesite) and scale up the application, the problem of agglomeration needs to be resolved. This will be investigated in the future.

■ AUTHOR INFORMATION

Corresponding Author

*E-mail: marzena.kwapinska@ul.ie.

Author Contributions

The manuscript was written through contributions of all authors. All authors have given approval to the final version of the manuscript.

Notes

The authors declare no competing financial interest.

■ ACKNOWLEDGMENTS

Financial support for this work is gratefully acknowledged and is provided by the Competence Centre for Biorefining & Biofuels as an Enterprise Ireland research grant (CC/2009/1305A). Gang Xue acknowledges the postgraduate grant received from Chinese Scholarship Council. Stephen Dooley is supported by Science Foundation Ireland under grant No. 799 06/CP/E007.

■ REFERENCES

- (1) BP Statistical Review of World Energy June 2012. bp.com/statisticalreview (accessed May 29, 2013).
- (2) Fryda, L. E.; Panopoulos, K. D. Agglomeration in fluidized bed gasification of biomass. *Powder Technol.* **2008**, *181*, 307–320.
- (3) Öhman, M.; Pommer, L.; Nordin, A. Bed agglomeration characteristics and mechanisms during gasification and combustion of biomass fuels. *Energy Fuels* **2005**, *19* (4), 1742–1748.
- (4) Alauddin, Z. A. B. Z.; Lahijani, P.; Mohammadi, M.; Mohamed, A. R. Gasification of lignocellulosic biomass in fluidized beds for renewable energy development: A review. *Renewable Sustainable Energy Rev.* **2010**, *14* (9), 2852–2862.
- (5) Rousset, P.; Aguiar, C.; Labb  , N.; Commandr  , J.-M. Enhancing the combustible properties of bamboo by torrefaction. *Bioresour. Technol.* **2011**, *102* (17), 8225–8231.
- (6) Bridgeman, T. G.; Jones, J. M.; Williams, A.; Waldron, D. J. An investigation of the grindability of two torrefied energy crops. *Fuel* **2010**, *89* (12), 3911–3918.
- (7) Michel, R.; Rapagn  , S.; Di Marcello, M.; Burg, P.; Matt, M.; Courson, C.; Gruber, R. Catalytic steam gasification of *Miscanthus X giganteus* in fluidized bed reactor on olivine based catalysts. *Fuel Process. Technol.* **2011**, *92* (6), 1169–1177.
- (8) Smoli  ski, A.; Sta  czyk, K.; Howaniec, N. Steam gasification of selected energy crops in a fixed bed reactor. *Renewable Energy* **2010**, *35* (2), 397–404.
- (9) Chen, G.; Spliethoff, H.; Andries, J.; Glazer, M. P.; Yang, L. B. Biomass gasification in a circulating fluidized bed—Part I: Preliminary experiments and modelling development. *Energy Sources* **2004**, *26* (5), 485–498.
- (10) Kallis, K. X.; Pellegrini Susini, G. A.; Oakey, J. E. A comparison between Miscanthus and bioethanol waste pellets and their performance in a downdraft gasifier. *Appl. Energy* **2013**, *101* (0), 333–340.
- (11) Siedlecki, M.; de Jong, W. Biomass gasification as the first hot step in clean syngas production process—Gas quality optimization and primary tar reduction measures in a 100 kW thermal input steam–oxygen blown CFB gasifier. *Biomass Bioenergy* **2011**, *35* (Supplement 1), S40–S62.
- (12) Siedlecki, M.; Nieuwstraten, R.; Simeone, E.; de Jong, W.; Verkooijen, A. H. M. Effect of magnesite as bed material in a 100 kWth steam–oxygen blown circulating fluidized-bed biomass gasifier on gas composition and tar formation. *Energy Fuels* **2009**, *23* (11), S643–S654.
- (13) Bartels, M.; Lin, W.; Nijenhuis, J.; Kapteijn, F.; van Ommen, J. R. Agglomeration in fluidized beds at high temperatures: Mechanisms, detection, and prevention. *Prog. Energy Combust. Sci.* **2008**, *34* (5), 633–666.
- (14) Liliedahl, T.; Sj  str  m, K.; Engvall, K.; Ros  n, C. Defluidization of fluidized beds during gasification of biomass. *Biomass Bioenergy* **2011**, *35* (Supplement 1), S63–S70.
- (15) Basile, F.; Albertazzi, S.; Barbera, D.; Benito, P.; Einval, J.; Brandin, J.; Fornasari, G.; Trifir  , F.; Vaccari, A. Steam reforming of hot gas from gasified wood types and Miscanthus biomass. *Biomass Bioenergy* **2011**, *35* (Supplement 1), S116–S122.
- (16) Hayes, D. J. M. Mass and compositional changes, relevant to biorefining, in *Miscanthus x giganteus* plants over the harvest window. *Bioresour. Technol.* **2013**, *142* (0), 591–602.

- (17) Sluiter, A.; B. H., Ruiz, R.; Scarlata, C.; ; Sluiter, J.; D. T.; Crocker, D. *Determination of Structural Carbohydrates and Lignin in Biomass* [electronic resource]: Laboratory Analytical Procedure (LAP); National Renewable Energy Laboratory: Golden, CO, 2008.
- (18) Basu, P. *Biomass Gasification and Pyrolysis: Practical Design and theory*; Elsevier: Amsterdam, 2010.
- (19) Yu, Y. *Mechanics of Fluidization*; West Virginia University: Morgantown, WV, 1965.
- (20) Basu, P. *Combustion and Gasification in Fluidized Beds*; CRC Press: Boca Raton, FL, 2006.
- (21) Gómez-Barea, A.; Arjona, R.; Ollero, P. Pilot-plant gasification of olive stone: A technical assessment. *Energy Fuels* 2004, 19 (2), 598–605.
- (22) Lahijani, P.; Zainal, Z. A. Gasification of palm empty fruit bunch in a bubbling fluidized bed: A performance and agglomeration study. *Bioresour. Technol.* 2011, 102 (2), 2068–2076.
- (23) Kaewluan, S.; Pipatmanomai, S. Potential of synthesis gas production from rubber wood chip gasification in a bubbling fluidized bed gasifier. *Energy Convers. Manage.* 2011, 52 (1), 75–84.
- (24) Manyà, J. J.; Sánchez, J. L.; Ábreo, J.; Gonzalo, A.; Arauzo, J. Influence of gas residence time and air ratio on the air gasification of dried sewage sludge in a bubbling fluidized bed. *Fuel* 2006, 85 (14–15), 2027–2033.
- (25) Eom, I.-Y.; Kim, J.-Y.; Lee, S.-M.; Cho, T.-S.; Yeo, H.; Choi, J.-W. Comparison of pyrolytic products produced from inorganic-rich and demineralized rice straw (*Oryza sativa* L.) by fluidized bed pyrolyzer for future biorefinery approach. *Bioresour. Technol.* 2013, 128 (0), 664–672.
- (26) Pinto, F.; Franco, C.; André, R. N.; Tavares, C.; Dias, M.; Gulyurtlu, I.; Cabrita, I. Effect of experimental conditions on co-gasification of coal, biomass and plastics wastes with air/steam mixtures in a fluidized bed system. *Fuel* 2003, 82 (15–17), 1967–1976.
- (27) Emami Taba, L.; Irfan, M. F.; Wan Daud, W. A. M.; Chakrabarti, M. H. The effect of temperature on various parameters in coal, biomass, and CO-gasification: A review. *Renewable Sustainable Energy Rev.* 2012, 16 (8), 5584–5596.
- (28) Ross, D.; Noda, R.; Horio, M.; Kosminski, A.; Ashman, P.; Mullinger, P. Axial gas profiles in a bubbling fluidized bed biomass gasifier. *Fuel* 2007, 86 (10–11), 1417–1429.
- (29) Arena U., D. G., F, Zaccariello L., Mastellone M. L. Fluidized bed gasification of biomass: A substance flow analysis. *The 13th International Conference on Fluidization—New Paradigm in Fluidization Engineering*, Gyeong-ju, Korea 2010.
- (30) Brus, E.; Ohman, M.; Nordin, A. Mechanisms of bed agglomeration during fluidized-bed combustion of biomass fuels. *Energy Fuels* 2005, 19 (3), 825–832.
- (31) Kuo, J.-H.; Lin, C.-L.; Wey, M.-Y. Effect of alkali concentrations and operating conditions on agglomeration/defluidization behavior during fluidized bed air gasification. *Powder Technol.* 2011, 214 (3), 443–446.
- (32) Lin, C.-L.; Wey, M.-Y. The effect of mineral compositions of waste and operating conditions on particle agglomeration/defluidization during incineration. *Fuel* 2004, 83 (17–18), 2335–2343.
- (33) Grimm, A.; Öhman, M.; Lindberg, T.; Fredriksson, A.; Boström, D. Bed agglomeration characteristics in fluidized-bed combustion of biomass fuels using olivine as bed material. *Energy Fuels* 2012, 26 (7), 4550–4559.
- (34) Skrifvars, B.-J.; Backman, R.; Hupa, M. Characterization of the sintering tendency of ten biomass ashes in FBC conditions by a laboratory test and by phase equilibrium calculations. *Fuel Process. Technol.* 1998, 56 (1–2), 55–67.
- (35) Vuthaluru, H. B.; Zhang, D.-k.; Linjewile, T. M. Behavior of inorganic constituents and ash characteristics during fluidized-bed combustion of several Australian low-rank coals. *Fuel Process. Technol.* 2000, 67 (3), 165–176.
- (36) Seville, J. P. K.; Willett, C. D.; Knight, P. C. Interparticle forces in fluidization: A review. *Powder Technol.* 2000, 113 (3), 261–268.
- (37) Valmari, T.; Tutkimuskeskus, V. T. *Potassium Behaviour during Combustion of Wood in Circulating Fluidised Bed Power Plants*; Technical Research Centre of Finland: VTT, Finland, 2000.
- (38) Vassilev, S. V.; Vassileva, C. G. A new approach for the combined chemical and mineral classification of the inorganic matter in coal. 1. Chemical and mineral classification systems. *Fuel* 2009, 88 (2), 235–245.